HHS Public Access

Author manuscript

Immunity. Author manuscript; available in PMC 2018 August 15.

Published in final edited form as:

Immunity. 2017 August 15; 47(2): 363–373.e5. doi:10.1016/j.immuni.2017.07.016.

Dendritic cells but not macrophages sense tumor mitochondrial DNA for cross-priming through signal regulatory protein α signaling

Meng Michelle Xu[1,2], **Yang Pu**[1], **Dali Han**[3], **Yaoyao Shi**[2], **Xuezhi Cao**[1], **Hua Liang**[2], **Xiang Chen**[4], **Xiao-Dong Li**[4], **Liufu Deng**[5], **Zhijian J. Chen**[4], **Ralph R. Weichselbaum**[2], and **Yang-Xin Fu**[1,6,*]

[1]Department of Pathology, University of Texas Southwestern Medical Center, Dallas, TX 75235, USA

[2]Department of Radiation and Cellular Oncology, The Ludwig Center for Metastasis Research, University of Chicago, Chicago, IL 60637, USA

[3]Department of Chemistry, Department of Biochemistry and Molecular Biology, and Institute for Biophysical Dynamics, Howard Hughes Medical Institute, University of Chicago, Chicago, IL 60637, USA

[4]Howard Hughes Medical Institute, University of Texas Southwestern Medical Center, Dallas, TX 75390, USA

[5]Shanghai Institute of Immunology, Shanghai Jiaotong University School of Medicine, Shanghai 200025, China

Summary

Inhibition of cytosolic DNA sensing represents a strategy that tumor cells use for immune evasion, but the underlying mechanisms are unclear. Here we have shown that CD47-signal regulatory protein α (SIRPα) axis dictates the fate of ingested DNA in DCs for immune evasion. Although macrophages were more potent in uptaking tumor DNA, increase of DNA sensing by blocking the interaction of SIRPα with CD47 preferentially occurred in dendritic cells (DCs), but not in macrophages. Mechanistically, CD47 blockade enabled the activation of NADPH oxidase NOX2 in DCs, which in turn inhibited phagosomal acidification and reduced the degradation of tumor mitochondrial DNA (mtDNA) in DCs. MtDNA was recognized by cyclic-GMP-AMP synthase (cGAS) in the DC cytosol, contributing to type I interferon (IFN) production and antitumor

*Correspondence: Yang-Xin.Fu@utsouthwestern.edu.
6Lead Contact: Yang-Xin Fu

Author contributions

Y. X.F and M.M.X conceived and designed the study; M. M.X., Y. P, and D.L.H, Y.S., H.L, and L.D. performed the experiments. X.C, X,-D.L., Z.J.C contributed resources. M. M.X. and D.L.H analyzed the data. M. M. X., Y. P, D.L.H, R.R.W, and Y. X.F, wrote the manuscript.

adaptive immunity. Thus, our findings have demonstrated how tumor cells inhibit innate sensing in DCs, and suggested that the CD47-SIRPα axis is critical for DC-driven antitumor immunity.

Introduction

As a central cytoplasmic DNA sensor upstream of STING (stimulator of interferon genes), cGAS has been shown to sense dsDNA and catalyze the generation of the secondary messenger cGAMP (cyclic GMP-AMP) during viral infection and lupus erythematosus (Barrat et al., 2016; Gao et al., 2015; Gao et al., 2013; Schoggins et al., 2014; Sun et al., 2013). cGAMP in turn binds to STING and triggers the downstream TBK1 kinase-IRF3 transcription factor axis (Gao et al., 2013; Sun et al., 2013). However, while the function of cGAS-mediated DNA sensing is well-established in antibacterial and antiviral immunity, the role of cGAS in antitumor immunity and the character of DNA that triggers such antitumor immune responses in anti-cancer therapies have not been extensively investigated. Recently, tumor derived double-stranded DNA (dsDNA) has been shown to be taken up by host antigen presenting cells (APC) and translocated into cytosol, similar to antigen up take (Deng et al., 2014; Michelle Xu et al., 2016; Sistigu et al., 2014; Woo et al., 2015). Cytosolic tumor DNA therefore triggers the DNA sensing STING pathway and contributes to the antitumor immune responses. However, whether and how engulfed tumor DNA is processed preferentially by selected phagocytes after initial phagocytosis are largely unknown.

CD47 is a transmembrane protein known as a “don’t eat me” signal that interacts with signal regulatory protein α (SIRPα) expressed on macrophages and dendritic cells (Barclay and Van den Berg, 2014; Blazar et al., 2001; Oldenborg et al., 2000). Engagement of SIRPα by CD47 promotes the phosphorylation of the ITIMs (immunoreceptor tyrosine-based inhibitory motif) in the cytoplasmic tail of SIRPα, which in turn recruits SHP-1 and/or SHP-2 [src homology-2 (SH2)-domain containing protein tyrosine phosphatases] to dephosphorylate motor protein myosin IIA and thereby inhibits phagocytosis. Accumulating evidence indicates that CD47 is expressed widely across multiple cancer types, and abundant CD47 has correlated with poor survival in several types of cancers (Chan et al., 2009; Jaiswal et al., 2009; Majeti et al., 2009; Rendtlew Danielsen et al., 2007). Moreover, the potential of blocking CD47-SIRPα interactions as a therapeutic target has been demonstrated in various preclinical models, which has led to multiple ongoing clinical trials (Chao et al., 2011a; Chao et al., 2010; Chao et al., 2011b; Tseng et al., 2013; Willingham et al., 2012). Therefore, the CD47 pathway might be required for optimal tumor-mediated immune evasion. While most preclinical mechanistic explorations highlighted the macrophage-dependent antitumor efficacy (Chao et al., 2011a; Weiskopf et al., 2016; Willingham et al., 2012), several studies intriguingly demonstrate that the therapeutic effect of CD47 blockade largely depends on DC cross-priming of $CD8^+$ T cells mediated by type I interferon (IFN)(Liu et al., 2015; Sockolosky et al., 2016; Tseng et al., 2013). Type I IFN has been identified as an essential component in the innate immune recognition of tumor, bridging the innate and adaptive immunity in cancer and various anti-cancer treatments. It has been shown that interruption of CD47-SIRPα signaling enables an increase of type I IFN exclusively in DC, in contrast to the minimal changes observed in macrophages (Liu et al., 2015). Such specialized function of DCs after tumor uptake cannot simply be explained

by its capacity for phagocytosis, since DCs are considered less potent than macrophage in engulfing tumor cells. It is unclear whether tumor restricts DNA sensing occurs differentially in DC versus macrophage after modifying CD47-SIRPα signaling and what downstream molecular cascade orchestrates the specialized capacity of DCs in generating type I IFN.

Here, we report that in contrast to macrophages, DCs are more specialized in utilizing cytosolic DNA sensing pathway to bridge innate response to adaptive response after anti-CD47-mediated phagocytosis. Upon CD47 blockade, tumor-originated mtDNA is phagocytosed by macrophages with a rapid degradation. In contrast, ingested mtDNA in DC is channeled into cytosolic compartment successfully, leading to cGAS-STING-IRF3-mediated cytosolic DNA sensing for tumor rejection.

Results

DCs are specialized in DNA sensing triggered by CD47 blockade

Most studies examined phagocytosis-associated tumor killing by utilizing macrophages due to their superior potency in phagocytosis. However, our recent study shows that DCs are more potent in their ability to generate type I IFNs and cytotoxic T lymphocytes (CTL) after CD47 blockade (Liu et al., 2015). To further address cellular requirement of DNA sensing in response to CD47 blockade, we crossed *Tmem173*$^{f/f}$ mice with *Lyz2*-cre to delete STING in mature macrophages, while using *Itgax-cre* to delete STING in DCs (Fig S1A) (Blaauboer et al., 2015; Jin et al., 2013). *Lyz2*-cre;*Tmem173*$^{f/f}$ mice rejected tumor cells as similar as *Tmem173*$^{f/f}$ mice after anti-CD47 treatment (Fig. 1A). In contrast, conditional deletion of STING in CD11c^{+} DCs completely abolished the antitumor effect of anti-CD47 mAb (Fig. 1B). These data demonstrate that in MC38 tumor model, therapeutic anti-CD47 preferentially relies on STING-mediated DNA sensing in DC, whereas intrinsic STING signaling in macrophage makes a minor contribution to the antitumor immunity during CD47-blockade.

The lack of DNA sensing in macrophages could be explained by a defect in CD47-blockade-mediated phagocytosis. To compare the phagocytic capacity of macrophages and DCs, we labeled MC38 cells with CFSE and co-cultured with bone marrow-derived DCs (BMDCs) or macrophages (BMMs). We observed that both DCs and macrophages displayed enhanced phagocytosis in response to CD47 blockade, while macrophages phagocytosed even more effectively than DCs (Fig. 1C). Consistently, an enhanced accumulation of DNA was detected inside both DCs and macrophage after CD47 blockade (Fig. 1D), indicating that the specialized function of DCs in DNA sensing cannot be attributed to its potency in capturing tumor-derived DNA. Given FcγR (Fcγ receptor) signals are demonstrated to trigger type I IFN production (Chao et al., 2010; Henault et al., 2012), we therefore examined whether FcγR with diverse expression pattern on different phagocytes contribute to the unique ability of DCs in DNA sensing. We found that both WT mice and *Fcer1g*$^{-/-}$ mice were able to control tumor growth after treatment with anti-CD47 mAb (Fig. 1 E–F). Consistently, inhibition of Fc binding to FcR did not change IFN-β induction in response to anti-CD47 mAb (Fig. S1B). Collectively, these data suggest therapeutic CD47 blockade relies on a

FcγR-independent DNA sensing signaling in DCs instead of macrophages, notwithstanding their similar capacities of engulfing tumor cells and uptaking tumor-derived DNA.

Tumor-derived mtDNA is preferentially increased in the cytosol of DCs, but not macrophage in response to CD47 blockade

The nature of DNA with selective access to particular DNA sensor could be critical for distinct outcomes of DNA sensing in different phagocytes. To explore whether the type of DNA released into cytosol dictates the unique ability of DCs for STING-mediated sensing, we quantified the component of cytosolic DNA content from BMDCs co-cultured with MC38 cells. Although a four-fold increase of both cytosolic gDNA (genomic DNA) and mtDNA (mitochondrial DNA) was observed in response to anti-CD47 treatment, we found a higher abundance of mtDNA fragments than gDNA inside the cytosol of *in vitro*-cultured BMDCs (Fig. S2A and Fig. 2A). In fact, gDNA was barely detectable in the cytosol of BMDCs when comparing with mtDNA. Because tumor cells cultured *in vitro* cannot completely recapitulate the tumor microenvironment *in vivo*, we therefore implanted MC38 tumor cells on the flanks of WT mice to study the impact of CD47 blockade inside tumor microenvironment. Consistent with our findings *in vitro*, an increased abundance of mtDNA was also detected in the cytosol of tumor-infiltrating DCs, whereas gDNA was rarely observed within the cytosol despite increasing after CD47 blockade (Fig. S2B and Fig. 2B), implying that enhanced enrichment of mtDNA could be a critical event determining the consequence of cytosolic DNA sensing in DCs. We next asked whether different cell types differ in their ability to generate cytosolic mtDNA in response to anti-CD47-mediated phagocytosis. While no significant change of mtDNA was observed in macrophages and monocytes, mtDNA was markedly increased in DCs in response to CD47 blockade in MC38 tumor model (Fig. 2C). These results suggest that CD47 blockade allows an accumulation of cytosolic mtDNA in DCs, which maybe a requirement for the effective innate sensing.

It is possible that the enhancement of mtDNA enriched in DC cytosol is released from endogenous stressed mitochondrial after blocking CD47-SIRPα signaling in DC. To test this, we used a mitochondrial-stress indicator MitoSOX to specifically detect superoxide in the mitochondria of DCs. Anti-CD47 did not increase the MitoSOX fluorescence in DCs (Fig. S2C), indicating increased cytosolic mtDNA may not be due to endogenous mitochondrial stress. To further confirm such cytosolic mtDNA is associated with ingested tumor cells but not from endogenous DNA in DCs, CD47-positive human colon cancer HCT116 was xenografted into NOD scid gamma (NSG) mice whose SIRPα is able to bind to human CD47 (Takenaka et al., 2007), therefore human DNA from transplanted tumor can be distinguished from recipient mouse DNA in DCs. While the amount of tumor and host gDNA was comparable in the cytosol of DCs, we observed an increase in the enrichment of tumor mtDNA as compared with host endogenous mtDNA after anti-CD47 treatment, reinforcing the conclusion that cytosolic DNA in DCs is mainly derived from ingested tumor mtDNA (Fig. 2D). Collectively, these data indicate that CD47 blockade promotes the accumulation of tumor-derived mtDNA in the cytosol of DCs, which might be an essential step triggering innate sensing in phagocytes.

Phagocytosed mitochondrial DNA is required for anti-CD47-mediated innate sensing in DCs

To assess the functional significance of tumor-derived mtDNA in DCs, we cultured MC38 tumor cells with dideoxycytidine (ddC) to generate mtDNA-depleted tumor cells (Fig. 3A). We observed a five-fold increase in the production of IFN-β in DCs isolated from parental but not from mtDNA-depleted MC38 three days after CD47 blockade, while IFN-β was not induced in tumor infiltrating macrophages (Fig. 3B). This data suggests that tumor-derived mtDNA is required for innate sensing in DCs triggered by CD47 blockade. We next determined whether reduced mtDNA could actually affect the ability of DCs to cross-prime $CD8^+$ T cells. The function of DCs to cross-present antigen was augmented by CD47 blockade when stimulated with parental tumor cells. However, reducing mtDNA in tumor cells abolished the ability of DCs to cross-prime T cells (Fig. 3C), which suggests that mtDNA from tumor cells is required for anti-CD47-mediated cross priming.

Given that ROS (reactive oxygen species)-mediated oxidation of DNA potentiates mtDNA access to the cytosol for subsequent immune-recognition (Caielli et al., 2016; Lood et al., 2016), we hypothesized that a greater amount of mtDNA elicited by ROS stress might strengthen the capacity of DCs to produce type I IFN upon anti-CD47 mAb treatment. To test this hypothesis, tumor cells were transiently pretreated with rotenone prior to incubation with BMDCs. In the context of rotenone treatment, we observed more potent IFN-β induction in BMDCs upon CD47 blockade (Fig. 3D), consistent with reports demonstrating the high pro-inflammatory properties of released oxidized mtDNA (Lood et al., 2016; Shimada et al., 2012; West et al., 2015). By using CRISPR/Cas9 genome editing, we generated a stable *Cd47*$^{-/-}$ variant of MC38 tumor cells (Fig. 3E). In comparison with the parental cells, *Cd47* ablation significantly repressed tumor growth *in vivo* (Fig. 3F). However, the inhibition of growth of *Cd47*$^{-/-}$ MC38 cells was markedly reversed when tumor mtDNA was depleted, indicating that tumor-derived mtDNA is essential for tumor control (Fig. 3F). Taken together, these data demonstrate that increased release of tumor mtDNA into cytosol is an essential upstream step to trigger cytosolic DNA sensing during CD47 blockade.

Blocking SIRPα signaling on DC prevents phagosomal acidification and inhibits DNA degradation

Oversupply of DNA or defects in the DNA-degradation can result in the increased activation of DNA sensing pathways. Given the potency of macrophage in phagocytosis, we thus speculated whether the degradation machinery in macrophage phagosomes favors faster clearance of phagocytosed mtDNA than DC. To test this, phagosomal DNA degradation was analyzed over different time points. Although CD47 blockade increased mtDNA in both DC and macrophage phagosomes, macrophages degraded engulfed mtDNA more efficiently than DCs did (Fig. 4A), suggesting a restriction of DNA degradation in DCs after anti-CD47 treatment in MC38 tumor model.

Effective fusion between phagosomes and lysosomes leads to a fast acidification of phagosomal lumen, which in turn activates lysosomal DNase II for DNA degradation (Peitsch et al., 1994). We found that, in contrast to DC, a higher proportion of macrophage

phagosome with lysosomal marker LAMP-1 was observed in macrophage (Fig. 4B), while a delayed acquisition of LAMP-1 was detected in DCs after CD47 blockade-mediated phagocytosis (Fig. 4B), indicating an unique role of CD47-SIRPα signaling in DC to regulate the phagosomal function. We next tested the phagosomal pH in DC and macrophages in response to CD47 blockade. Consistently, pH in DC phagosomes acidified slower than macrophage in the absence of anti-CD47 (Fig. 4C–D). While the phagosomal environment in macrophages was not significantly changes after blocking CD47-SIRPα signaling (Fig. 4C), CD47 blockade was able to prevent phagosomal acidification in DCs (Fig. 4D). In addition, inhibiting phagosomal acidification with chloroquine further improved the efficiency of DNA sensing in DCs and allowed macrophage gain DNA sensing after CD47 blockade (Fig. S3A and Fig. S3B). Together, these data suggest that intervention of CD47-SIRPα signaling in DCs specifically modified the phagosomal environment less favorable state for degradation.

Blocking SIRPα signaling on DC phagosomes induces a NOX2-dependent decrease in degradation of engulfed DNA

We next asked how SIRPα signaling in DCs interacts with the pathways regulating phagosome function. Compared with macrophages, DCs have developed a specialized phagocytic pathway to maintain the alkaline pH in phagosomes via recruiting NOX2 to the phagosomal membrane, where NOX2 produces ROS to consume protons generated by V-ATPase and delay the acidification of phagosomal lumen (Mantegazza et al., 2008; Savina et al., 2006). We observed that while no enhancement of ROS was found in macrophages, a higher amount of phagosomal ROS was found in DCs after blocking CD47-SIRPα signaling (Fig. 5A). The generation of ROS was markedly inhibited in phagosomes from gp91^{phox}(Nox2)-deficient DCs, confirming that functional NOX2 is essential for phagosomal ROS in DCs after CD47 blockade (Fig. 5B). In addition, CD47 blockade did not increases the expression of NOX2 (Fig. S4A). We reasoned that the SIRPα signaling might directly control the activity of NOX2 on DC phagosomes. The activation of NOX2 is dependent on tyrosine phosphorylation of p47^{phox}, while binding of CD47 to SIRPα on DC is shown to recruit the tyrosine phosphatase SHP-1 (Chowdhury et al., 2005; Ding et al., 2016; Oldenborg et al., 2001). Therefore, we sought to examine whether p47^{phox} could be the de-phosphorylation target of SIRPα-SHP-1. Co-immunoprecipitation showed that p47^{phox} interacted with SIRPα and SHP-1 in DCs. Less SHP-1 and SIRPα were observed following CD47 blockade, while tyrosine-phosphorylation of p47^{phox} was greater in DCs upon anti-CD47 mAb treatment (Fig. 5C). In contrast, tyrosine-phosphorylation of p47^{phox} was not changed in macrophages after anti-CD47 mAb treatment, suggesting that the activity of NOX2 in BMDM is controlled independent of CD47-SIRPα signaling (Fig. S4B). Collectively, these results indicate that engagement of SIRPα by CD47 recruits SHP-1 to dephosphorylate p47^{phox}, and consequently inhibit the activation of NOX2. Furthermore, the greater activity of NOX2 in DCs could be restored by CD47 blockade. To confirm the critical role of NOX2 in regulating DNA sensing, we compared the amount of cytosolic mtDNA in WT and gp91^{phox}(Nox2)-deficient DCs or macrophages upon CD47 blockade. While no change of cytosolic mtDNA was observed in both WT and gp91^{phox}(Nox2)-deficient macrophages, cytosolic mtDNA was significantly decreased in gp91^{phox}(Nox2)-deficient DCs during CD47 blockade-mediated phagocytosis (Fig. 5D). Moreover, IFN-α

mRNA was decreased in gp91^{phox}(Nox2)-deficient BMDCs in comparison with WT BMDCs (Fig. S5A). Furthermore, tumor growth was inhibited in WT mice after CD47 blockade, while absence of host NOX2 significantly impaired the anti-CD47 mAb-mediated antitumor effect (Fig. S5B). Together, these results demonstrate that as a prerequisite for efficient immune recognition of tumor DNA, NOX2 in DC phagosomes is tightly controlled by SIRPα signaling to maintain cytosolic DNA amounts below the threshold of innate sensing. Alleviation of restriction on NOX2 in DCs by CD47 blockade generates sufficient engulfed tumor mtDNA for innate sensing, which contributes to successful antitumor response.

Mitochondrial DNA is increasingly sensed by cGAS after CD47 treatment

To determine whether tumor mtDNA ingested into the cytosol in response to anti-CD47 treatment could be directly recognized by cGAS in DCs, we co-incubated cGAS-expressing DC2.4 with tumor cells in the presence of anti-CD47 mAb for eight hours. Purified DC2.4 cells were subsequently cross-linked and immunoprecipitated with anti-FLAG mAb (Fig. 6A). A significant enrichment for mtDNA, but not gDNA, was detected when cells were treated with anti-CD47 mAb (Fig. 6A). To ensure that the association of mtDNA-cGAS was not attributed to an over expression artifact, we examined whether endogenous cGAS of DCs could interact with mtDNA upon CD47 blockade. Consistently, mtDNA, but not gDNA, was significantly enriched in the endogenous cGAS immunoprecipitate after anti-CD47 mAb treatment as compared to rat Ig control, confirming that mtDNA in the cytosol was directly bound by cGAS (Fig. 6B).

To further assess the origin of cGAS-bound DNA, human tumor cells were co-cultured with BMDCs from NSG mice. While the amount of tumor-derived or host-derived gDNA was not changed after CD47 blockade (Fig. 6C), tumor-derived mtDNA was enriched five-fold in the anti-CD47-treated mice. Even though a low amount of host mtDNA was detected binding to cGAS, mtDNA originated from tumor cells was the predominant DNA source with enhanced binding to cGAS after anti-CD47 mAb treatment (Fig. 6C). Together, these data suggest that mtDNA from tumor cells binds to and activates cGAS in host DC cells in response to CD47 blockade.

cGAS signaling controls type I IFN induction by DCs upon CD47 blockade

We next determined whether cGAS (encoded by Mb21d1) is required for DC sensing of tumor cells as a potential opportunity, upstream of STING, to cross-prime antigen-specific CTL response. Our results indicated that the cross-priming capacity of DCs was enhanced by the stimulation of tumor cells in the presence of anti-CD47 mAb (Fig. 7A). However, cGAS-deficient BMDCs were unable to cross-prime antigen-specific CD8$^+$ T cells efficiently in response to anti-CD47 mAb (Fig. 7A). Consistently, the induction of IFN-β was significantly abrogated in the absence of cGAS in response to CD47 blockade (Fig. 7B). Given that the activation of cGAS-STING promotes type I IFN transcription via Tbk1 kinase-Irf3 transcription factor signaling axis (Sun et al., 2013), we examined whether anti-CD47 mAb treatment could induce phosphor-IRF3 *in vivo*. Indeed, anti-CD47 mAb enhanced the activation of IRF3 in tumor-infiltrating DCs one day after treatment (Fig. S6). Similar to cGAS-deficient BMDCs, IFN-β production and CTL cross-priming were severely

impaired in IRF3-deficient DCs, further confirming the necessity of this pathway for DC activation by anti-CD47mAb (Fig. 7C–D). To test the possibility that mtDNA-mediated cGAS activation can also occur in human primary DCs, we cultured human DCs with tumor cell line HCT116. Indeed, mtDNA was increased inside the cytosol of DC after CD47 blockade and IFN-β transcripts were enhanced in human DCs (Fig. S7). Furthermore, cGAS mRNA expression was significantly up-regulated in human DC after anti-CD47 treatment (Fig.S7), suggesting that DNA sensing may trigger a positive feedback loop through amplifying cGAS-mediated signaling. Collectively, these data indicate that anti-CD47 mAb treatment triggers cGAS-STING-IRF3-mediated type I IFN production.

cGAS is required for tumor rejection after anti-CD47 treatment

To further assess the critical role of cGAS in host immune cells in response to anti-CD47 treatment, we inoculated MC38 or B16-SIY tumor cells on the flanks of mice reconstituted with either wild-type or *Mb21d1*$^{-/-}$ bone marrow. We observed that the antitumor effect of anti-CD47 mAb is dramatically abolished in mice reconstituted with *Mb21d1*-WT bone marrow cells (BMC), whereas tumor burden was significantly reduced by anti-CD47 mAb in WT-WT reconstituted mice. The result indicated that the bone marrow derived cell expressing cGAS is essential for an anti-CD47 mAb-mediated antitumor effect (Fig. 7E–F). We also measured tumor growth in Irf3-deficient mice. As compared to WT mice, tumors grew faster in Irf3-deficient hosts upon CD47 blockade, suggesting that the cGAS-STING-IRF3 axis is required for anti-CD47-mediated tumor control (Fig. 7G). Consistent with previous observations, anti-CD47 mAb can elicit effective tumor antigen-specific CD8$^+$ T cell responses in WT mice, whereas the tumor-specific CD8$^+$ T cell responses in cGAS-deficient mice after CD47 blockade were diminished (Fig. 7H). Together, these data demonstrate that the host cGAS pathway plays a critical role in T cell priming and the therapeutic efficacy of anti-CD47 mAb therapy.

Discussion

Cytosolic DNA sensing is essential for the induction of type I IFNs and cross-priming. However, whether and how different type of phagocytes functions distinctively for processing engulfed DNA is largely unclear. Since macrophages are more potent in phagocytosis than DC, one would expect that macrophages can uptake more DNA for better innate sensing. However, we observed that preventing the engagement of SIRPα by CD47 promoted DNA sensing selectively in DCs, but not in macrophages. We showed that 1) although CD47 blockade increases phagocytosis of tumor cells by both macrophages and DCs, the therapeutic effect of anti-CD47 mAb largely depended on cytosolic DNA sensing pathway in DCs; 2) mtDNA was uniquely maintained in DC phagosomes and released into DC cytosol; 3) Reduced mtDNA from tumor cells impaired type I IFN production and cross-priming of DCs; 4) In addition to enhancing phagocytosis, intervention of SIRPα signaling on DCs by anti-CD47 Ab prevented the clearance of engulfed mtDNA by activating NOX2; 5) Tumor mtDNA directly interacted with cGAS in the cytosol of DCs; 6) The cGAS-STING-IRF3 signaling pathway was required for anti-CD47 mAb to generate type I IFN and cross-prime CD8$^+$ T cells; 7) Activation of the cGAS pathway was essential for the antitumor effect of anti-CD47 mAb.

Macrophages and DC are professional phagocytic cells that are able to recognize and uptake pathogens, dying cells and malignant cell very efficiently. However, the specialization of each population for processing engulfed DNA to initiate innate sensing is still unclear. In CD47 blockade-mediated phagocytosis, we observed that the antigen presenting cell (APC) commitment to immunogenic innate sensing was regulated by a specific phagocytic program adapted by DC, but not macrophages. In contrast to macrophages, DCs could maintain an alkaline phagosomal lumen by NOX2 to delay DNA degradation. However, such a mechanism was demonstrated to be insignificant in macrophages. It is possible that the rapid assembly of V-ATPase in phagosome enables a rapid rise in the concentration of H^+ within minutes after phagocytosis, but NOX2 in macrophages is insufficient to counteract the phagosomal acidification (Lukacs et al., 1990; Mantegazza et al., 2008; Savina et al., 2006). Therefore, the ingested DNA can be rapidly and completely degraded in macrophage phagosomes. In addition, macrophages have higher expression of DNase II that allows them to completely digest tumor DNA without activating DNA sensing pathway (Kawane et al., 2001). Macrophages lacking DNase II cannot eliminate engulfed DNA and develop an inflammatory disease, which is rescued by loss of STING function (Ahn et al., 2012). This suggests that the macrophage is more adapted to destroy the ingested DNA in order to prevent the development of autoimmunity. Together, our study has now demonstrated that in addition to its superior capacity in antigen processing and presentation, the DC is specialized in opening the cytosolic DNA sensing pathway under control of CD47-SIRPα axis, thus coordinately contributing to the activation of adaptive immune system.

Unlike the relatively well-demonstrated mechanism governing the cytosolic DNA sensing pathway in antibacterial and antiviral immunity, the role of tumor-derived DNA in cytosolic DNA sensing for cancer initiation or anti-cancer therapies had not been well defined. We and others have provided evidence suggesting that activation of STING and type I IFN production are particularly critical for innate immune sensing of tumor cells (Deng et al., 2014; Woo et al., 2014). However, which type of DNA, mtDNA or gDNA, is the dominant DNA required for innate sensing remained to be determined. Our results have revealed that mtDNA binding to cGAS is upstream of the STING pathway and is essential to the efficacy of therapeutic CD47 blockade. The critical function of mtDNA has been mostly studied in infection (West et al., 2015). More recently, the release of oxidized mtDNA with potent interferongenic properties has been observed during NETosis (Neutrophil extracellular traps) and caspase-inhibited apoptosis (Caielli et al., 2016; Laguette et al., 2014; Lood et al., 2016; Rongvaux et al., 2014). Once mtDNA enters into the cytoplasm, it might initiate interferon production via the DNA sensor cGAS, a process similar to that employed by foreign bacterial and viral DNA (Chen et al., 2016; Wu and Chen, 2014). Our study does not exclude that gDNA can efficiently bind to cGAS, but rather it demonstrates that mtDNA is a major initiator of antitumor immunity as a result of anti-CD47 mediated phagocytosis. It has been shown that, in tumor cells undergo massive apoptosis and necrosis, gDNA can then become fragmented and contribute to innate sensing (Lan et al., 2014; Shen et al., 2015).

Identification of tumor-derived DNA as the inducer for innate sensing raises the question of how DNA is released into the cytosol of host APCs and interacts with DNA sensors after CD47 blockade. One possibility is through binding to the antimicrobial peptide LL37, which leads to resistance to DNase II degradation and escape from autophagic recognition

(Chamilos et al., 2012; Zhang et al., 2015). Another possibility is that tumor-derived DNA may be transferred through gap junctions composed of connexin 43 (CX43) in a contact-dependent manner, which is known to regulate several immunological processes such as antigen cross-presentation (Neijssen et al., 2005). Additionally, it is tempting to speculate that ROS generated during phagocytosis can oxidize DNA originating from tumor-facilitating its escape from phagosomes (Gehrke et al., 2013; Lood et al., 2016). This is a possibility since mtDNA is more vulnerable to oxidative damage as compared with gDNA, due to a lack of protection by histones. Thus, it would be of interest to dissect the underlying mechanism responsible for the entrance of tumor-originated mtDNA into the cytosol of host APCs.

In this study, we observed that higher amount of CD47 on tumor can inhibit DNA sensing in DC for immune evasion. In addition to reducing “do not eat me” signaling, the principal antitumor effect of anti-CD47 mAb is attributed to the activation of mtDNA-mediated host cGAS-STING pathway inside DCs. The combination of anti-CD47 mAb with “eat me signaling” enhancers, such as genotoxic agents, including radiotherapy and chemotherapy as well as targeted therapies, could be a potential therapeutic strategy to synergistically enhance phagocytosis and trigger mtDNA sensing to improve the adaptive immune response.

STAR Methods

• CONTACT FOR REAGENT AND RESOURCE SHARING

Further information and requests for reagents should be directed to and will be fulfilled by the Lead Contact, Yang-Xin Fu (Yang-Xin.Fu@utsouthwestern.edu)

• EXPERIMENTAL MODEL AND SUBJECT DETAILS

Mice—Six- to eight-weeks old female C57BL/6J mice, Balb/c mice, CD45.1 mice, *gp91*$^{phox-/-}$ mice and NOD-scid IL2R$\gamma^{-/-}$(NSG) mice were purchased from Jackson laboratory. *Fcer1g*$^{-/-}$ mice were purchased from Taconic. *Mb21d1*$^{-/-}$ mice were kindly provided by Dr. Zhijian J. Chen of University of Texas Southwestern Medical Center. *Irf3*$^{-/-}$ mice were kindly provided by Dr. T. Taniguchi of University of Tokyo. *Tmem173*$^{f/f}$ mice were kindly provided by Dr. John C Cambier, of University of Colorado Denver and National Jewish Health. *Tmem173*$^{f/f}$ mice were crossed to either *Lyz2*-cre-Tg (Jackson laboratory) or *Itgax*-cre-Tg (Jackson laboratory) to obtain the conditional deficient mice. All the mice were maintained under specific pathogen-free conditions and used in accordance with the animal experimental guidelines set by the Institute of Animal Care and Use Committee. This study has been approved by the Institutional Animal Care and Use Committee of The University of Chicago.

Cell lines—MC38 is a murine colon adenocarcinoma cell line. A20 is a murine lymphoma cell line. B16F10 is a murine malignant melanoma cell line. MC38-SIY was selected for a single clone after being transduced by lentivirus expressing human EGFR (L858R)-SIY. B16-SIY melanoma cells were obtained from Dr. Thomas Gajewski (The University of Chicago). B16-OVA is an OVA-transfected clone derived from the murine melanoma cell line B16. DC2.4 cells were the immature dendritic cells of C57BL/6 mice. HCT116 is a

human colon cancer cell line. All the cell lines were tested to be mycoplasma free. To generate mtDNA-depleted cells, ddC (Sigma) was re-suspended in DMSO and added to cell culture at a final concentration of 50μM, and replenished every 48 h. Cells were maintained either in DMEM (Invitrogeon) supplemented with 10% FBS and 1% penicillin-streptomycin or RPMI 1640 (Invitrogen) supplemented with 2 mM L-glutamine, 1 mM sodium pyruvate, 0.1 mM nonessential amino acid, 1% penicillin-streptomycin, 2-ME, and 10% FBS at 37°C in 5% CO_2.

Primary cell cultures—Single-cell suspensions of bone marrow cells were cultured in RPMI-1640 medium containing 10% fetal bovine serum, supplemented with 20ng/ml GM-CSF for BMDC and 20ng/ml M-CSF for BMM (Peprotech). Fresh media with GM-CSF or M-CSF was added into culture on day 3. For induction of human DCs, human peripheral blood mononuclear cells (STEMCELL) were cultured in the presence of 40ng/ml human GM-CSF (Biolegend) and 40ng/ml human IL-4 (Biolegend). CD11c+ DCs were sorted after seven days.

• METHOD DETAILS

Reagents and Construct—Anti-mouse CD47 blocking mAb (clone MIAP301) and anti-human CD47 blocking mAb (clone B6H12) were purchased from Bio×cell (West Lebanon, NH). EdU was purchased from Invitrogen. Conjugated antibodies against CD11b, CD11c, Ly6C, CD45, F4/80 and CD45 were purchased from BioLegend. pcDNA3.1-Flag-mouse cGAS plasmid was kindly provided by Dr. Zhijian J. Chen of University of Texas Southwestern Medical Center.

DNA uptake assay—MC38 cells were incubated with EdU (10μM) overnight in complete DMEM culture medium. 2×10^6 bone marrow-derived dendritic cells or macrophage were plated in a 6-well ultra-low-adherent plate (Corning) and cultured with 2×10^6 EdU labeled cancer cells (MC38) in 2% FBS RPMI medium. Rat Ig or anti-CD47 antibody (30μg/mL) was added and incubated for 4 h at 37°. The percentage of phagocytosed DNA was ca lculated as the percentage of EdU^+ cells within DCs or macrophages.

Phagocytosis assay—MC38 cells were labled with 5uM CFSE (Biolegend) and co-cultured with BMDC or BMM for one hour in a 96-well ultra-low-adherent plate. Rat Ig or anti-CD47 antibody (30μg/mL) was added and incubated for 4 h at 37°. Cells were stained with anti-CD45 and analyzed using a BD LSR Fortessa Analyzer.

Tumor Growth and Treatments—1×10^6 MC38 or B16-SIY tumor cells were subcutaneously injected into the flank of mice. Tumors were allowed to grow for 9–14 days and were treated by anti-mouse CD47 mAb or rat Ig intratumorally. 3×10^6 A20 tumor cells were subcutaneously injected into the flank of mice. Tumors were allowed to grow for 12 days and treated by anti-mouse CD47 mAb or rat Ig intratumorally. 1×10^6 HCT116 human cancer cells were subcutaneously injected into the flank of NSG mice. Tumors were allowed to grow for 14 days and treated by anti-human CD47 mAb or mouse Ig intratumorally. Tumor volumes were measured by length (a) and width (b) and calculated as tumor volume = $ab^2/2$.

Tumor digestion—Tumor tissues were excised and digested with 1mg/ml Collagenase D (Sigma), 100mg/ml DNase I (Sigma) in the incubator with 5% CO_2. After 30 minutes, tumor was then passed through a 70μm cell strainer to remove large pieces of undigested tumor. Tumor infiltrating cells were washed twice with PBS containing 2 mM EDTA.

Flow Cytometric Sorting and Analysis—Single cell suspensions were blocked with anti-FcR (clone 2.4G2, Bio×cell) and then stained with antibodies against CD11c (Clone N418), CD11b (Clone M1/70), Ly6C (Clone HK1.4), F4/80 (Clone BM8) and CD45 (Clone 30-F11). Cells were sorted on a FACS Aria II Cell Sorter (BD). For pIRF3 staining, single cell suspensions were stained with CD11c and CD45, and permeabilized with the Fixation/ Permeabilization kit (eBioscience). Cells were then stained with pIRF3 antibody (CST, Cat # 29047) intracellularlly followed by anti-rabbit IgG-PE secondary antibody (Thermo Fisher Scientific). Data were analyzed with FlowJo Software (TriStar).

Generation of CD47$^{-/-}$ MC38—To introduce DSBs, 1×10^5 MC38 tumor cells were transfected with a CRISPR ribonucleoprotein (RNP) complex, containing Alt-R CRISPR crRNA:tracrRNA and Cas9 nuclease, according to the manufacturer's protocol (Lonza). CD47 negative cells were sorted by FACS two days after transfection. For targeting mouse CD47, the following sgCD47 sequence was used: sgCD47 5'-CCTTGCATCGTCCGTAATG-3' (Weiskopf et al., 2016).

Detection of DNA in cytosolic extracts—10^6 of purified DCs were divided into two equal aliquots, and one aliquot was lysed in 100 μl of 50 μM NaOH and boiled for 15 min (West et al., 2015). These whole cell lysates were neutralized with 10ul of 1 M Tris-HCl pH 8 (10×), which served as normalization controls for total DNA. The other equal aliquots were resuspended in 100 μl cytosolic extract buffer containing 150 mM NaCl, 50 mM HEPES and 25 μg/ml digitonin (Sigma) and incubated for 10 min on ice for plasma membrane permeabilization (West et al., 2015). Then cells were centrifuged to pellet intact cells. The cytosolic supernatants were collected and centrifuged at maximal speed for 10 min to pellet the remaining cellular debris. DNA from whole cell lysates or cytosolic extract was subjected to protease K for 1 hour and purified using DNA Clean & Concentrator (ZYMO RESEARCH). Quantitative PCR was performed on both whole-cell extracts and cytosolic fractions using gDNA primers and mtDNA primers. gDNA/mtDNA CT values obtained from the cytosolic fractions were normalized to gDNA abundance for whole-cell extracts to control the variations in cell number among samples.

Phagosomal DNA degradation and phago-lysosomal fusion—DCs or macrophages were pulsed with 3-μm magnetic beads and co-cultured with MC38 in the presence of 30μg/ml rat Ig or anti-CD47. After one hour, DCs or macrophages were sorted by FACS. The phagosomes were purified on indicated time points and the copy number of phagosomal DNA was detected by real-time PCR. To detect phago-lysosomal fusion, purified phagosomes were stained with anti-LAMP1(Biolegend) and measured by flow cytometry (Savina et al., 2010).

Detection of phagosomal NOX2 activity and PH—3-μm amino spheres were covalently coupled to dihydrorhodamine 123 (DHR) (Santa Cruz) and Alexa Fluor 647 (Life

Technologies) in NaHCO3 buffer (pH 8.5) for 2 h at room temperature (Ding et al., 2016). Beads were then washed twice with PBS. BMDCs or BMMs were pulsed with the DHR-coupled beads for 15 min, washed with cold PBS, chased for one hour, and analyzed by flow cytometry. Variation in DHR MFI was then determined. To measure phagosomal PH, 3-μm amino spheres (Polyscience) were coupled to 1 mg/ml 1 mg/ml Alexa Fluor 647 (Life Technologies) and FITC (Sigma-Aldrich) in NaHCO3 buffer (pH 8.5) for 2 h at room temperature. Beads were washed and resuspended in PBS. Cells were pulsed with beads in CO2-independent medium for 15 min at 37 °C and then washed with cold PBS. The ratio of the MFI emission between the two dyes was analyzed by flow cytometry at the indicated time points and was normalized to the standard curve obtained by cells incubated in a fixed-pH solution (ranging from pH 5.5 to pH 8.0) containing 0.1% Triton X-100.

***In vitro* function assay of BMDCs—**BMDCs or BMMs were harvested for stimulation assay on day 7. BMDCs were added and co-cultured with tumor cells at the ratio of 1:1 in the presence of fresh GM-CSF with 30μg/ml anti-CD47 antibody or rat Ig. To detect mitochondrial stress, cells were stained with anti-CD11c and mitoSOX (Life Technologies). For FcγR blockade, 10μg/ml 2.4G2 was added into cell culture and incubated overnight. For rotenone (Abcam) treatment, MC38 cells were pre-treated with 1μM rotenone for two hours. For chloroquine treatment, tumor cells were co-cultured with BMDC or BMDM in the presence of 5μM chloroquine (Invivogen). Subsequently, purified $CD11c^+$ cells were either tested for type I IFN production or incubated with isolated $CD8^+$ T cells from naive OT-I mice or 2C mice at the ratio of 1:10 for 2–3 days. IFN-β was detected by Mouse IFN Beta ELISA Kit (PBL Assay Science). IFNα/β transcripts were determined by real-time PCR. IFN-γ production was either detected by IFN-γ Flex Set CBA assay (BD Bioscience) or Elispot assay (BD Bioscience).

RT-PCR analysis of type I IFN—Total RNA from sorted cells was extracted with the RNeasy Micro Kit (QIAGEN) and reversed-transcribed with Seniscript Reverse Transcription Kit (QIAGEN). Real-time RT-PCR was performed with SSoFast EvaGreen supermix (Bio-Rad) according to the manufacturer's instructions and different primer sets on StepOne Plus (Applied Biosystems). Data were normalized by the amount of reference gene in each individual sample. The $2^{-\Delta\Delta Ct}$ method was used to calculate relative expression changes.

Measurement of IFN γ-Secreting $CD8^+$ T Cells by ELISPOT Assay—For tumor-specific $CD8^+$ T cell functional assay in the MC38 model, 10 days after anti-CD47 Ab treatment, $CD8^+$ T cells were purified from spleen. 2.5×10^5 $CD8^+$ T cells were re-stimulated with MC38 cells at the ratio of 20:1 for 48 hours. 96-well HTS-IP plate (Millipore) was pre-coated with anti-IFN-γ antibody (BD Bioscience) with a 1:250 dilution overnight at 4° C. After co-culture, cells were removed. 2μg/ml biotinylated anti-IFN-γ antibody (BD Bioscience) with a 1:250 dilution was added and incubated for 2h at room temperature or overnight at 4°C. Avidin-horseradish peroxidase (BD Bioscience) with a 1:1000 dilution was then added and the plate was incubated for 1h at room temperature. The cytokine spots of IFN-γ were developed according to product protocol (BD Bioscience).

T cell isolation—OT-I naïve $CD8^+$ T cells or 2C naïve $CD8^+$ T cells were isolated from lymph nodes and spleen of 6 to 12-week-old mice. Selection was carried out with a negative CD8 isolation kit (Stemcell Technologies) following manufacturer's instruction.

Coimmunoprecipitation—BMDCs and BMDMs were added and co-cultured with MC38 cells at the ratio of 1:1 in the presence of 30μg/ml anti-CD47 antibody or rat Ig for three hours. BMDCs were stained with anti-CD11c and sorted by FACS. BMDMs were stained with anti-CD11b and sorted by FACS. Cells were lysed with cell-lysis buffer (Cell Signaling Technology) supplemented with a protease inhibitor cocktail (Calbiochem). Immunoprecipitation was performed with p47phox (D-10, Santa Cruz) for four hours at 4°C. Protein G beads was added and incubated for 1 hour at 4°C. Immunoprecipitates were washed five times with 1× lysis buffer. The phosphorylated tyrosine in the p47phox subunit was detected using antibody to P-Tyr-1000 (Cell Signaling Technology) after immunoprecipitation of p47phox. Antibody to SHP-1 (C-19) was obtained from Santa Cruz. Antibody to SIRPα(P84) was obtained from Millipore. HRP-linked antibody to rabbit IgG, HRP-linked antibody to rat IgG and HRP-linked antibody to mouse IgG were obtained from Santa Cruz.

Immunoprecipitation-PCR—DC2.4 transduced with an expression plasmid (pcDNA3.1) encoding Flag-tagged mouse cGAS were co-cultured with MC38 and treated with rat Ig or anti-CD47 mAb for 8 hours. Following crosslinking of DNA and associated proteins, immunoprecipitation was performed with anti-FLAG M2 (Sigma) or mouse-IgG (biolegend) following manufacturer's instruction (Sigma). Co-precipitated DNA was examined by real-time qPCR. To pull-down endogenous cGAS, purified BMDCs were fixed for 10 min in 4% PFA and quenched with 1 M Tris pH 7.4 for 5 min. Fixed cells were washed and lysed in 50 mM Tris pH 7.4, 150 mM NaCl, 1 mM EDTA, 0.1% NP-40, and 1.25% Triton X-100 with 10 cycles of 30s sonication in BioRuptor water bath sonicator. Cell lysates were pre-cleared with protein A magnetic beads (Invitrogen) and immunoprecipitated using anti-mouse cGAS (CST) or rabbit Ig (CST) at 4°C overnight. Protein A beads was added and incubated for 1 hour at 4°C. Immunoprecipitates were washed five times with 50 mM Tris, 150 mM NaCl, 1 mM EDTA, and 0.05% NP-40 (Wash Buffer). Eluted DNA were reverse cross-linked and treated with 0.2 mg/ml proteinase K (Sigma) for 2 h at 37°C. DNA were extracted with ChIP DNA Clean & Concentrator™(ZYMO RESEARCH). DNA pellets were re-suspended and used in qPCR analysis to measure the abundance of specific DNA sequences.

Generation of bone marrow chimeras—$CD45.1^+$ WT mice were lethally irradiated with a single dose of 1000 rads. The next day irradiated mice were adoptively transferred with $2–3\times10^6$ bone marrow cells collected from $CD45.2^+cGAS^{-/-}$ or $CD45.2^+$WT mice. Mice were maintained on sulfamethoxazole and trimethoprim (Bactrim) antibiotics diluted in drinking water for 5 weeks after reconstitution. Mice were injected with tumor cells 5–6 weeks post-reconstitution.

• QUANTIFICATION AND STATISTICAL ANALYSIS

No statistical method was used to predetermine sample size. Mice were assigned at random to treatment groups for all mouse studies and, where possible, mixed among cages.

Whenever possible, the investigators were blinded to group allocation during the experiment and when assessing the outcome. Experiments were repeated two to three times. Data were analyzed using Prism 5.0 Software (GraphPad) and presented as mean values ± SEM. The p values were assessed using two-tailed unpaired Student's t test with p values considered significant as follows: *$p < 0.05$; **$p < 0.01$ and ***$p < 0.001$.

Supplementary Material

Refer to Web version on PubMed Central for supplementary material.

Acknowledgments

We thank Amy Huser and Daryl Harmon for excellent editing. This work was in part supported by the U.S. National Cancer Institute grants CA141975 and the Cancer Prevention and Research Institute of Texas to Y.X.F.

References

Ahn J, Gutman D, Saijo S, Barber GN. STING manifests self DNA-dependent inflammatory disease. Proceedings of the National Academy of Sciences of the United States of America. 2012; 109:19386–19391. [PubMed: 23132945]

Barclay AN, Van den Berg TK. The interaction between signal regulatory protein alpha (SIRPalpha) and CD47: structure, function, and therapeutic target. Annual review of immunology. 2014; 32:25–50.

Barrat FJ, Elkon KB, Fitzgerald KA. Importance of Nucleic Acid Recognition in Inflammation and Autoimmunity. Annual review of medicine. 2016; 67:323–336.

Blaauboer SM, Mansouri S, Tucker HR, Wang HL, Gabrielle VD, Jin L. The mucosal adjuvant cyclic di-GMP enhances antigen uptake and selectively activates pinocytosis-efficient cells in vivo. eLife. 2015; 4

Blazar BR, Lindberg FP, Ingulli E, Panoskaltsis-Mortari A, Oldenborg PA, Iizuka K, Yokoyama WM, Taylor PA. CD47 (integrin-associated protein) engagement of dendritic cell and macrophage counterreceptors is required to prevent the clearance of donor lymphohematopoietic cells. The Journal of experimental medicine. 2001; 194:541–549. [PubMed: 11514609]

Caielli S, Athale S, Domic B, Murat E, Chandra M, Banchereau R, Baisch J, Phelps K, Clayton S, Gong M, et al. Oxidized mitochondrial nucleoids released by neutrophils drive type I interferon production in human lupus. The Journal of experimental medicine. 2016; 213:697–713. [PubMed: 27091841]

Chamilos G, Gregorio J, Meller S, Lande R, Kontoyiannis DP, Modlin RL, Gilliet M. Cytosolic sensing of extracellular self-DNA transported into monocytes by the antimicrobial peptide LL37. Blood. 2012; 120:3699–3707. [PubMed: 22927244]

Chan KS, Espinosa I, Chao M, Wong D, Ailles L, Diehn M, Gill H, Presti J Jr, Chang HY, van de Rijn M, et al. Identification, molecular characterization, clinical prognosis, and therapeutic targeting of human bladder tumor-initiating cells. Proceedings of the National Academy of Sciences of the United States of America. 2009; 106:14016–14021. [PubMed: 19666525]

Chao MP, Alizadeh AA, Tang C, Jan M, Weissman-Tsukamoto R, Zhao F, Park CY, Weissman IL, Majeti R. Therapeutic antibody targeting of CD47 eliminates human acute lymphoblastic leukemia. Cancer research. 2011a; 71:1374–1384. [PubMed: 21177380]

Chao MP, Alizadeh AA, Tang C, Myklebust JH, Varghese B, Gill S, Jan M, Cha AC, Chan CK, Tan BT, et al. Anti-CD47 antibody synergizes with rituximab to promote phagocytosis and eradicate non-Hodgkin lymphoma. Cell. 2010; 142:699–713. [PubMed: 20813259]

Chao MP, Tang C, Pachynski RK, Chin R, Majeti R, Weissman IL. Extranodal dissemination of non-Hodgkin lymphoma requires CD47 and is inhibited by anti-CD47 antibody therapy. Blood. 2011b; 118:4890–4901. [PubMed: 21828138]

Chen Q, Sun L, Chen ZJ. Regulation and function of the cGAS-STING pathway of cytosolic DNA sensing. Nat Immunol. 2016; 17:1142–1149. [PubMed: 27648547]

Chowdhury AK, Watkins T, Parinandi NL, Saatian B, Kleinberg ME, Usatyuk PV, Natarajan V. Src-mediated tyrosine phosphorylation of p47phox in hyperoxia-induced activation of NADPH oxidase and generation of reactive oxygen species in lung endothelial cells. J Biol Chem. 2005; 280:20700–20711. [PubMed: 15774483]

Deng L, Liang H, Xu M, Yang X, Burnette B, Arina A, Li XD, Mauceri H, Beckett M, Darga T, et al. STING-Dependent Cytosolic DNA Sensing Promotes Radiation-Induced Type I Interferon-Dependent Antitumor Immunity in Immunogenic Tumors. Immunity. 2014; 41:843–852. [PubMed: 25517616]

Ding Y, Guo Z, Liu Y, Li X, Zhang Q, Xu X, Gu Y, Zhang Y, Zhao D, Cao X. The lectin Siglec-G inhibits dendritic cell cross-presentation by impairing MHC class I-peptide complex formation. Nat Immunol. 2016; 17:1167–1175. [PubMed: 27548433]

Gao D, Li T, Li XD, Chen X, Li QZ, Wight-Carter M, Chen ZJ. Activation of cyclic GMP-AMP synthase by self-DNA causes autoimmune diseases. Proceedings of the National Academy of Sciences of the United States of America. 2015; 112:E5699–5705. [PubMed: 26371324]

Gao P, Ascano M, Wu Y, Barchet W, Gaffney BL, Zillinger T, Serganov AA, Liu Y, Jones RA, Hartmann G, et al. Cyclic [G(2',5')pA(3',5')p] is the metazoan second messenger produced by DNA-activated cyclic GMP-AMP synthase. Cell. 2013; 153:1094–1107. [PubMed: 23647843]

Gehrke N, Mertens C, Zillinger T, Wenzel J, Bald T, Zahn S, Tuting T, Hartmann G, Barchet W. Oxidative damage of DNA confers resistance to cytosolic nuclease TREX1 degradation and potentiates STING-dependent immune sensing. Immunity. 2013; 39:482–495. [PubMed: 23993650]

Henault J, Martinez J, Riggs JM, Tian J, Mehta P, Clarke L, Sasai M, Latz E, Brinkmann MM, Iwasaki A, et al. Noncanonical autophagy is required for type I interferon secretion in response to DNA-immune complexes. Immunity. 2012; 37:986–997. [PubMed: 23219390]

Jaiswal S, Jamieson CH, Pang WW, Park CY, Chao MP, Majeti R, Traver D, van Rooijen N, Weissman IL. CD47 is upregulated on circulating hematopoietic stem cells and leukemia cells to avoid phagocytosis. Cell. 2009; 138:271–285. [PubMed: 19632178]

Jin L, Getahun A, Knowles HM, Mogan J, Akerlund LJ, Packard TA, Perraud AL, Cambier JC. STING/MPYS mediates host defense against Listeria monocytogenes infection by regulating Ly6C(hi) monocyte migration. Journal of immunology. 2013; 190:2835–2843.

Kawane K, Fukuyama H, Kondoh G, Takeda J, Ohsawa Y, Uchiyama Y, Nagata S. Requirement of DNase II for definitive erythropoiesis in the mouse fetal liver. Science. 2001; 292:1546–1549. [PubMed: 11375492]

Laguette N, Bregnard C, Hue P, Basbous J, Yatim A, Larroque M, Kirchhoff F, Constantinou A, Sobhian B, Benkirane M. Premature activation of the SLX4 complex by Vpr promotes G2/M arrest and escape from innate immune sensing. Cell. 2014; 156:134–145. [PubMed: 24412650]

Lan YY, Londono D, Bouley R, Rooney MS, Hacohen N. Dnase2a deficiency uncovers lysosomal clearance of damaged nuclear DNA via autophagy. Cell reports. 2014; 9:180–192. [PubMed: 25284779]

Liu X, Pu Y, Cron K, Deng L, Kline J, Frazier WA, Xu H, Peng H, Fu YX, Xu MM. CD47 blockade triggers T cell-mediated destruction of immunogenic tumors. Nature medicine. 2015; 21:1209–1215.

Lood C, Blanco LP, Purmalek MM, Carmona-Rivera C, De Ravin SS, Smith CK, Malech HL, Ledbetter JA, Elkon KB, Kaplan MJ. Neutrophil extracellular traps enriched in oxidized mitochondrial DNA are interferogenic and contribute to lupus-like disease. Nature medicine. 2016; 22:146–153.

Lukacs GL, Rotstein OD, Grinstein S. Phagosomal acidification is mediated by a vacuolar-type H(+)-ATPase in murine macrophages. J Biol Chem. 1990; 265:21099–21107. [PubMed: 2147429]

Majeti R, Chao MP, Alizadeh AA, Pang WW, Jaiswal S, Gibbs KD Jr, van Rooijen N, Weissman IL. CD47 is an adverse prognostic factor and therapeutic antibody target on human acute myeloid leukemia stem cells. Cell. 2009; 138:286–299. [PubMed: 19632179]

Mantegazza AR, Savina A, Vermeulen M, Perez L, Geffner J, Hermine O, Rosenzweig SD, Faure F, Amigorena S. NADPH oxidase controls phagosomal pH and antigen cross-presentation in human dendritic cells. Blood. 2008; 112:4712–4722. [PubMed: 18682599]

Michelle Xu M, Pu Y, Weichselbaum RR, Fu YX. Integrating conventional and antibody-based targeted anticancer treatment into immunotherapy. Oncogene. 2016

Neijssen J, Herberts C, Drijfhout JW, Reits E, Janssen L, Neefjes J. Cross-presentation by intercellular peptide transfer through gap junctions. Nature. 2005; 434:83–88. [PubMed: 15744304]

Oldenborg PA, Gresham HD, Lindberg FP. CD47-signal regulatory protein alpha (SIRPalpha) regulates Fcgamma and complement receptor-mediated phagocytosis. The Journal of experimental medicine. 2001; 193:855–862. [PubMed: 11283158]

Oldenborg PA, Zheleznyak A, Fang YF, Lagenaur CF, Gresham HD, Lindberg FP. Role of CD47 as a marker of self on red blood cells. Science. 2000; 288:2051–2054. [PubMed: 10856220]

Peitsch MC, Mannherz HG, Tschopp J. The apoptosis endonucleases: cleaning up after cell death? Trends Cell Biol. 1994; 4:37–41. [PubMed: 14731864]

Rendtlew Danielsen JM, Knudsen LM, Dahl IM, Lodahl M, Rasmussen T. Dysregulation of CD47 and the ligands thrombospondin 1 and 2 in multiple myeloma. British journal of haematology. 2007; 138:756–760. [PubMed: 17760807]

Rongvaux A, Jackson R, Harman CC, Li T, West AP, de Zoete MR, Wu Y, Yordy B, Lakhani SA, Kuan CY, et al. Apoptotic caspases prevent the induction of type I interferons by mitochondrial DNA. Cell. 2014; 159:1563–1577. [PubMed: 25525875]

Savina A, Jancic C, Hugues S, Guermonprez P, Vargas P, Moura IC, Lennon-Dumenil AM, Seabra MC, Raposo G, Amigorena S. NOX2 controls phagosomal pH to regulate antigen processing during cross-presentation by dendritic cells. Cell. 2006; 126:205–218. [PubMed: 16839887]

Savina A, Vargas P, Guermonprez P, Lennon AM, Amigorena S. Measuring pH, ROS production, maturation, and degradation in dendritic cell phagosomes using cytofluorometry-based assays. Methods Mol Biol. 2010; 595:383–402. [PubMed: 19941126]

Schoggins JW, MacDuff DA, Imanaka N, Gainey MD, Shrestha B, Eitson JL, Mar KB, Richardson RB, Ratushny AV, Litvak V, et al. Pan-viral specificity of IFN-induced genes reveals new roles for cGAS in innate immunity. Nature. 2014; 505:691–695. [PubMed: 24284630]

Shen YJ, Le Bert N, Chitre AA, Koo CX, Nga XH, Ho SS, Khatoo M, Tan NY, Ishii KJ, Gasser S. Genome-derived cytosolic DNA mediates type I interferon-dependent rejection of B cell lymphoma cells. Cell reports. 2015; 11:460–473. [PubMed: 25865892]

Shimada K, Crother TR, Karlin J, Dagvadorj J, Chiba N, Chen S, Ramanujan VK, Wolf AJ, Vergnes L, Ojcius DM, et al. Oxidized mitochondrial DNA activates the NLRP3 inflammasome during apoptosis. Immunity. 2012; 36:401–414. [PubMed: 22342844]

Sistigu A, Yamazaki T, Vacchelli E, Chaba K, Enot DP, Adam J, Vitale I, Goubar A, Baracco EE, Remedios C, et al. Cancer cell-autonomous contribution of type I interferon signaling to the efficacy of chemotherapy. Nature medicine. 2014; 20:1301–1309.

Sockolosky JT, Dougan M, Ingram JR, Ho CC, Kauke MJ, Almo SC, Ploegh HL, Garcia KC. Durable antitumor responses to CD47 blockade require adaptive immune stimulation. Proceedings of the National Academy of Sciences of the United States of America. 2016; 113:E2646–2654. [PubMed: 27091975]

Sun L, Wu J, Du F, Chen X, Chen ZJ. Cyclic GMP-AMP synthase is a cytosolic DNA sensor that activates the type I interferon pathway. Science. 2013; 339:786–791. [PubMed: 23258413]

Takenaka K, Prasolava TK, Wang JC, Mortin-Toth SM, Khalouei S, Gan OI, Dick JE, Danska JS. Polymorphism in Sirpa modulates engraftment of human hematopoietic stem cells. Nature immunology. 2007; 8:1313–1323. [PubMed: 17982459]

Tseng D, Volkmer JP, Willingham SB, Contreras-Trujillo H, Fathman JW, Fernhoff NB, Seita J, Inlay MA, Weiskopf K, Miyanishi M, Weissman IL. Anti-CD47 antibody-mediated phagocytosis of cancer by macrophages primes an effective antitumor T-cell response. Proceedings of the National Academy of Sciences of the United States of America. 2013; 110:11103–11108. [PubMed: 23690610]

Weiskopf K, Jahchan NS, Schnorr PJ, Cristea S, Ring AM, Maute RL, Volkmer AK, Volkmer JP, Liu J, Lim JS, et al. CD47-blocking immunotherapies stimulate macrophage-mediated destruction of

small-cell lung cancer. The Journal of clinical investigation. 2016; 126:2610–2620. [PubMed: 27294525]

West AP, Khoury-Hanold W, Staron M, Tal MC, Pineda CM, Lang SM, Bestwick M, Duguay BA, Raimundo N, MacDuff DA, et al. Mitochondrial DNA stress primes the antiviral innate immune response. Nature. 2015; 520:553–557. [PubMed: 25642965]

Willingham SB, Volkmer JP, Gentles AJ, Sahoo D, Dalerba P, Mitra SS, Wang J, Contreras-Trujillo H, Martin R, Cohen JD, et al. The CD47-signal regulatory protein alpha (SIRPa) interaction is a therapeutic target for human solid tumors. Proceedings of the National Academy of Sciences of the United States of America. 2012; 109:6662–6667. [PubMed: 22451913]

Woo SR, Corrales L, Gajewski TF. Innate immune recognition of cancer. Annual review of immunology. 2015; 33:445–474.

Woo SR, Fuertes MB, Corrales L, Spranger S, Furdyna MJ, Leung MY, Duggan R, Wang Y, Barber GN, Fitzgerald KA, et al. STING-dependent cytosolic DNA sensing mediates innate immune recognition of immunogenic tumors. Immunity. 2014; 41:830–842. [PubMed: 25517615]

Wu J, Chen ZJ. Innate immune sensing and signaling of cytosolic nucleic acids. Annual review of immunology. 2014; 32:461–488.

Zhang Z, Meng P, Han Y, Shen C, Li B, Hakim MA, Zhang X, Lu Q, Rong M, Lai R. Mitochondrial DNA-LL-37 Complex Promotes Atherosclerosis by Escaping from Autophagic Recognition. Immunity. 2015; 43:1137–1147. [PubMed: 26680206]

Highlights

- DCs are specialized in DNA sensing through regulation of SIRPα signaling
- Tumor-derived mtDNA is selectively increased in the cytosol of DCs after anti-CD47
- Blocking SIRPα signaling on DCs limits the degradation of mtDNA
- cGAS-mediated sensing triggered by mtDNA is required for anti-CD47 therapy

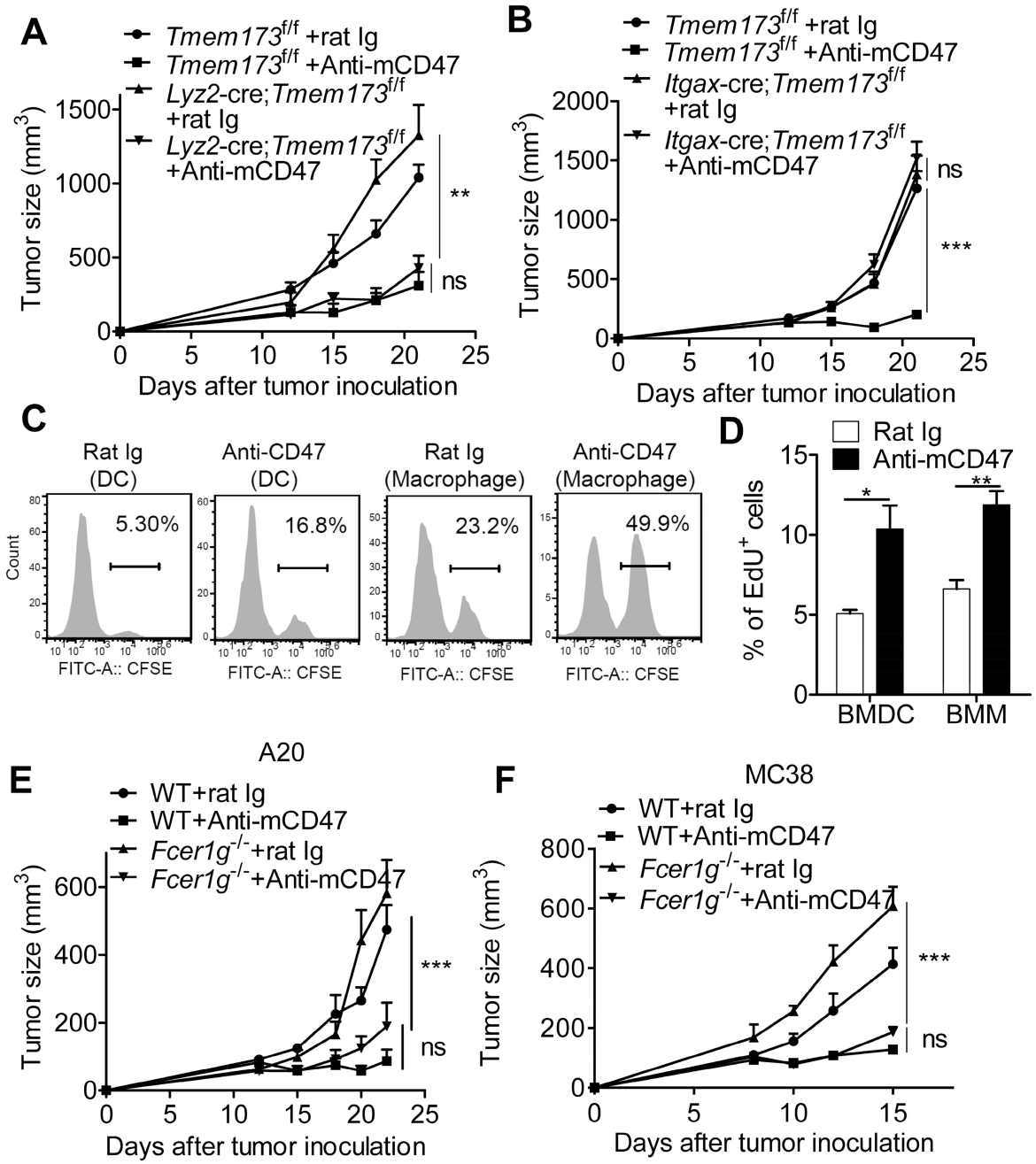

Figure 1. The therapeutic effect of anti-CD47 mAb depends on cytosolic DNA sensing pathway in DCs, but not in macrophage

(A–B) *Tmem173*$^{fl/fl}$ (n=5), *Lyz2*-cre;*Tmem173*$^{fl/fl}$ mice (n = 5) and *Itgax*-cre;*Tmem173*$^{fl/fl}$ mice (n = 5) were injected s.c. with 1 × 10^6 MC38 cells and treated with 50 μg of anti-CD47 or rat Ig on days 12 and 15. **(C)** CFSE-labeled MC38 tumor cells were co-cultured with bone marrow-derived DCs (BMDC) or macrophages (BMM) for one hour in the presence of 30μg/ml rat Ig or anti-CD47 mAb. **(D)** EdU-labeled MC38 tumor cells were co-cultured with BMDC or BMM for four hours in the presence of 30μg/ml rat Ig or anti-CD47 mAb. Percentage of EdU positive BMDC and BMM were quantified. **(E)** WT mice or *Fcer1g*$^{-/-}$

mice (n = 5 mice/group) were injected s.c. with 3×10^6 A20 cells and treated i.t. with 50 μg of anti-CD47 or rat Ig on days 12 and 15. **(F)** WT mice or *Fcer1g*$^{-/-}$ mice (n = 5 mice/group) were injected s.c. with 1×10^6 MC38 cells and treated i.t. with 50 μg of anti-CD47 or rat Ig on days 8 and 10. Data are representatives of two (A, B, E and F) or three (C, D) independent experiments and presented as mean ± SEM. * $p< 0.05$, ** $p< 0.01$, *** $p< 0.001$ (Two-tailed student's t test). See also Figure S1.

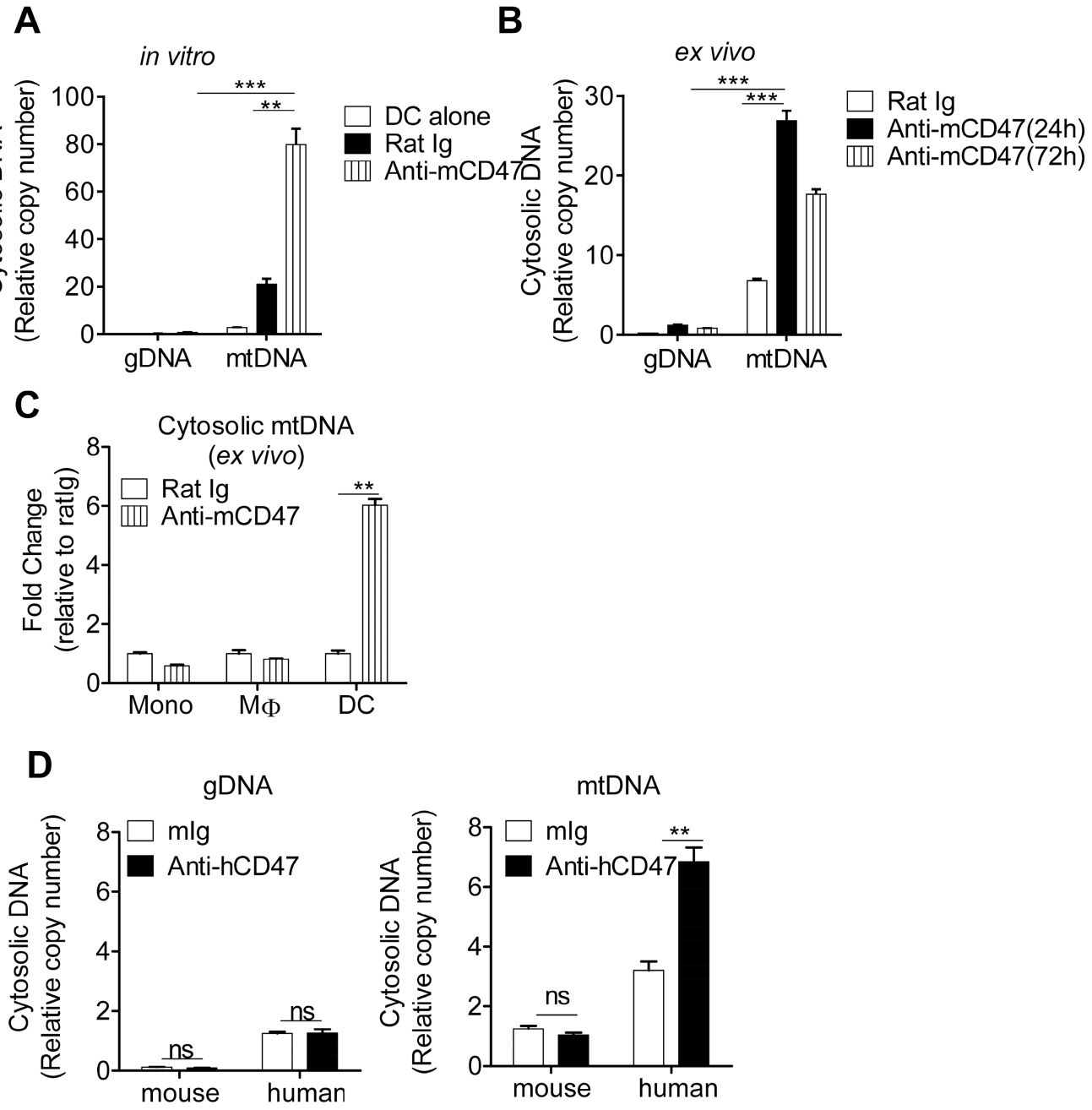

Figure 2. Tumor mtDNA is selectively increased inside the cytosol of DCs in response to CD47 blockade

(A) BMDCs were co-cultured with MC38 in the presence of rat Ig or anti-CD47 mAb for four hours. $CD11c^+$ DCs were purified and cytosolic DNA was extracted and quantitated via qPCR using the primer specific for genomic (*Polg1*) or mitochondrial DNA(*nd1*). **(B)** C57BL/6 mice were injected s.c. with 1×10^6 MC38 cells and treated i.t. with 50 μg of anti-CD47 mAb or isotype control rat Ig on day 12. 24 to 72 hours after anti-CD47 mAb or rat Ig treatment, DCs were sorted from tumors. Cytosolic amount of mtDNA and gDNA were quantitated by real-time PCR assay. **(C)** MC38 cells were injected s.c. into C57BL/6 mice. Tumor-bearing mice were treated i.t. with 50 μg of anti-CD47 or rat Ig on day 12. Two days

after treatment, the single-cell suspensions from tumors were sorted into monocytes, macrophages and DCs. **(D)** NSG mice were injected s.c. with 1×10^6 HCT116 cells and treated i.t. with 50 μg of anti-human CD47 mAb (clone B6H12) or isotype control mouse Ig on day 14. 24 hours after anti-human CD47 or mouse Ig treatment, DCs were sorted from tumors. Cytosolic amount of mtDNA and gDNA that originated from host (mouse DNA) or tumor cells (human DNA) were quantitated and normalized to mouse gDNA and mtDNA respectively obtained from the whole-cell extract. Data are represented as mean ± SEM after normalizing to the copy number of gDNA obtained from the whole-cell extract. * $p< 0.05$, ** $p< 0.01$, *** $p< 0.001$, ns, not significant (Two-tailed student's t test). Data are representative of two (C–D) or three (A–B) independent experiments. See also Figure S2.

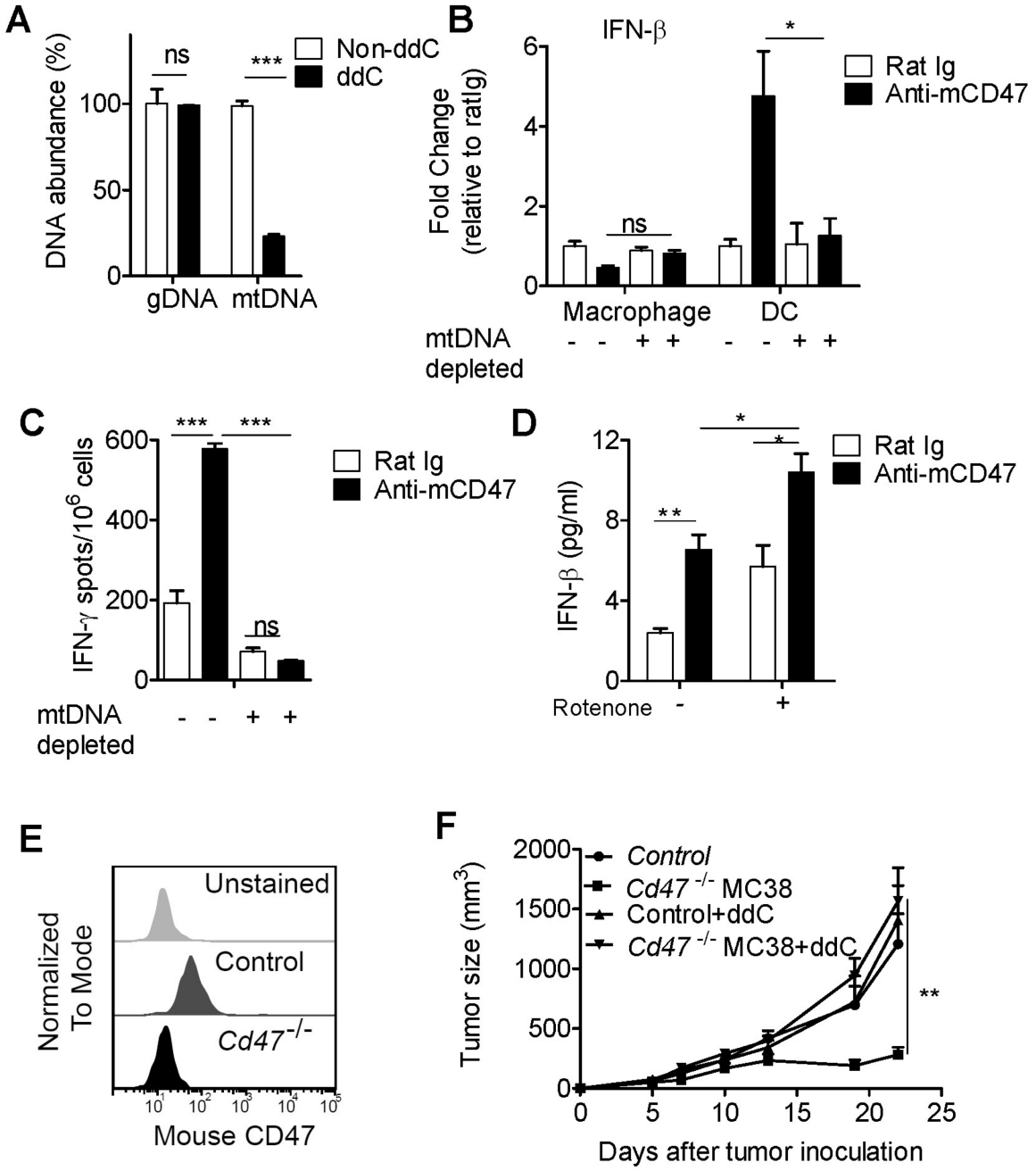

Figure 3. Tumor mtDNA is required for type I IFN production and cross-priming in DC

(A) mtDNA content from MC38 tumor cells cultured with ddC to generate mtDNA-depleted cells. **(B)** Mitochondrial DNA-depleted MC38 cells or parental MC38 cells were injected s.c. into C57BL/6 mice in the presence of rat Ig or anti-CD47 mAb. Three days after injection, the single-cell suspensions from tumors were sorted into macrophages and DCs. mRNA amount IFN-β in two cell subsets were quantified. Results are normalized to the amount of reference gene *Hprt* in three independent experiments. **(C)** BMDCs were cultured with mtDNA-depleted B16-OVA in the presence of anti-CD47 or rat Ig for 16 hours. Subsequently, purified $CD11c^+$ cells were co-cultured with isolated $CD8^+$ T cells from naive

OTI mice for two days. IFN-γ production was enumerated by ELISPOT. **(D)** BMDCs were cultured with 1μM rotenone-treated MC38 or non-treated MC38 in the presence of anti-CD47 or rat Ig for eight hours. ELISA assays for the concentration of IFN-β were performed. **(E)** Using CRISPR/Cas9 genome editing, *Cd47*$^{-/-}$ MC38 was generated. CD47 expression on the surface of parental MC38 cells (control) or *Cd47*$^{-/-}$ MC38 cells were analyzed by flow cytometry Unstained MC38 cell was used as a negative control. **(F)** Mitochondrial DNA-sufficient or depleted cells were injected s.c. into C57BL/6 mice (n=4 mice/group). Data are represented as mean ± SEM. *p< 0.05, **p< 0.01, **p< 0.001. ns, not significant (Two-tailed student's t test). Data are representative of two (D–F) or three (A–C) independent experiments.

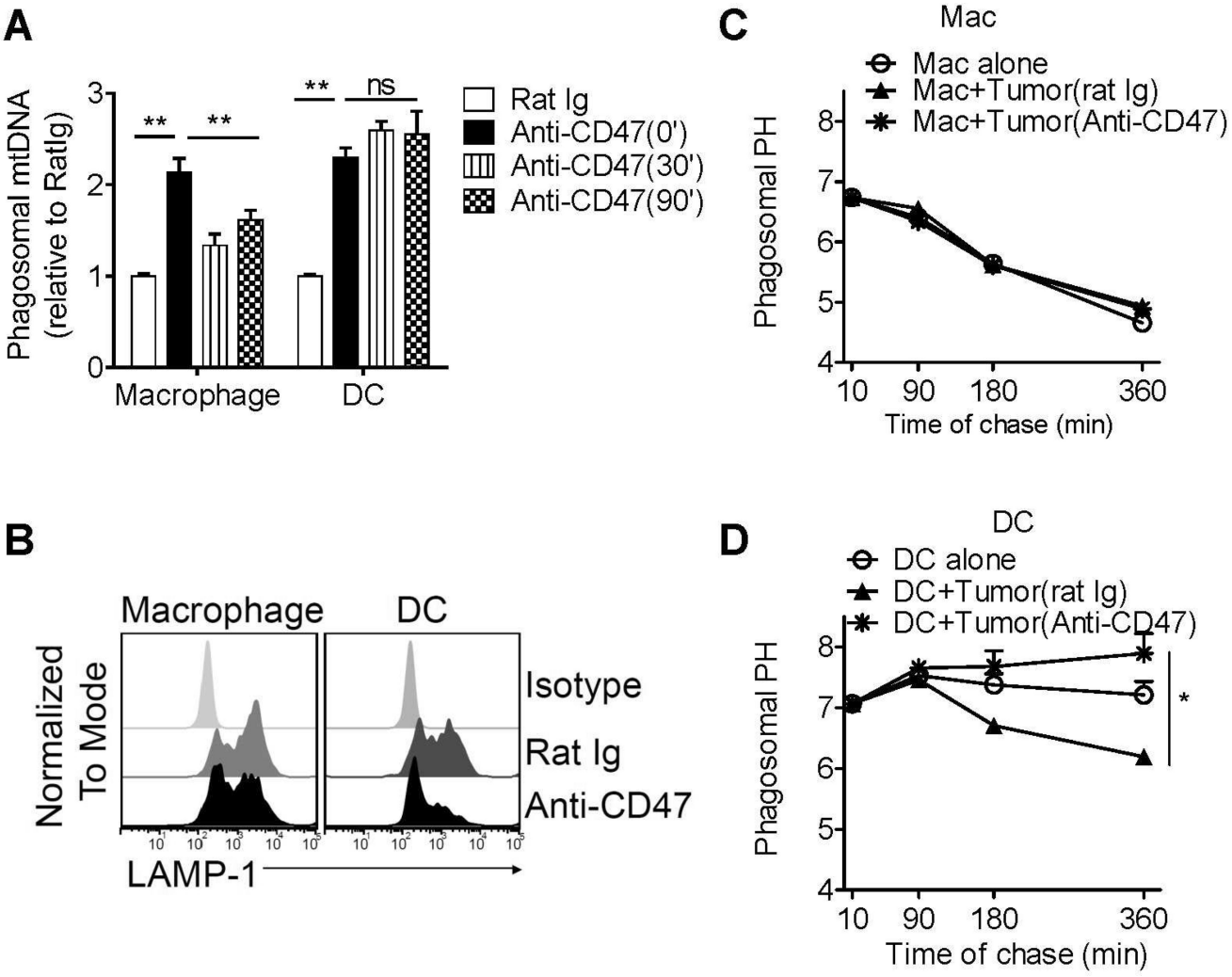

Figure 4. CD47-SIRPα signaling in DCs controls the phagosomal PH and DNA degradation

(A) MC38 tumor cells were co-cultured with bone marrow-derived DCs or macrophages in the presence of 30μg/ml rat Ig or anti-CD47 mAb. After one hour, $CD11c^+$ DCs or $F4/80^+$ macrophages were sorted. Phagosomal mtDNA was quantitated after different chase periods. **(B)** MC38 tumor cells were co-cultured with bone marrow-derived DCs or macrophages in the presence of 30μg/ml rat Ig or anti-CD47 mAb for one hour. Phagosomal acquisition of LAMP-1 was analyzed by flow organellocytometry. **(C–D)** BMDC and BMM were were cultured with MC38 tumor cells in the presence of rat Ig or anti-CD47 mAb. Phagosomal PH was measure on indicated time points. Data are represented as mean ± SEM. *$p< 0.05$, **$p< 0.01$. ns, not significant (Two-tailed student's t test). Data are representative of two independent experiments. See also Figure S3.

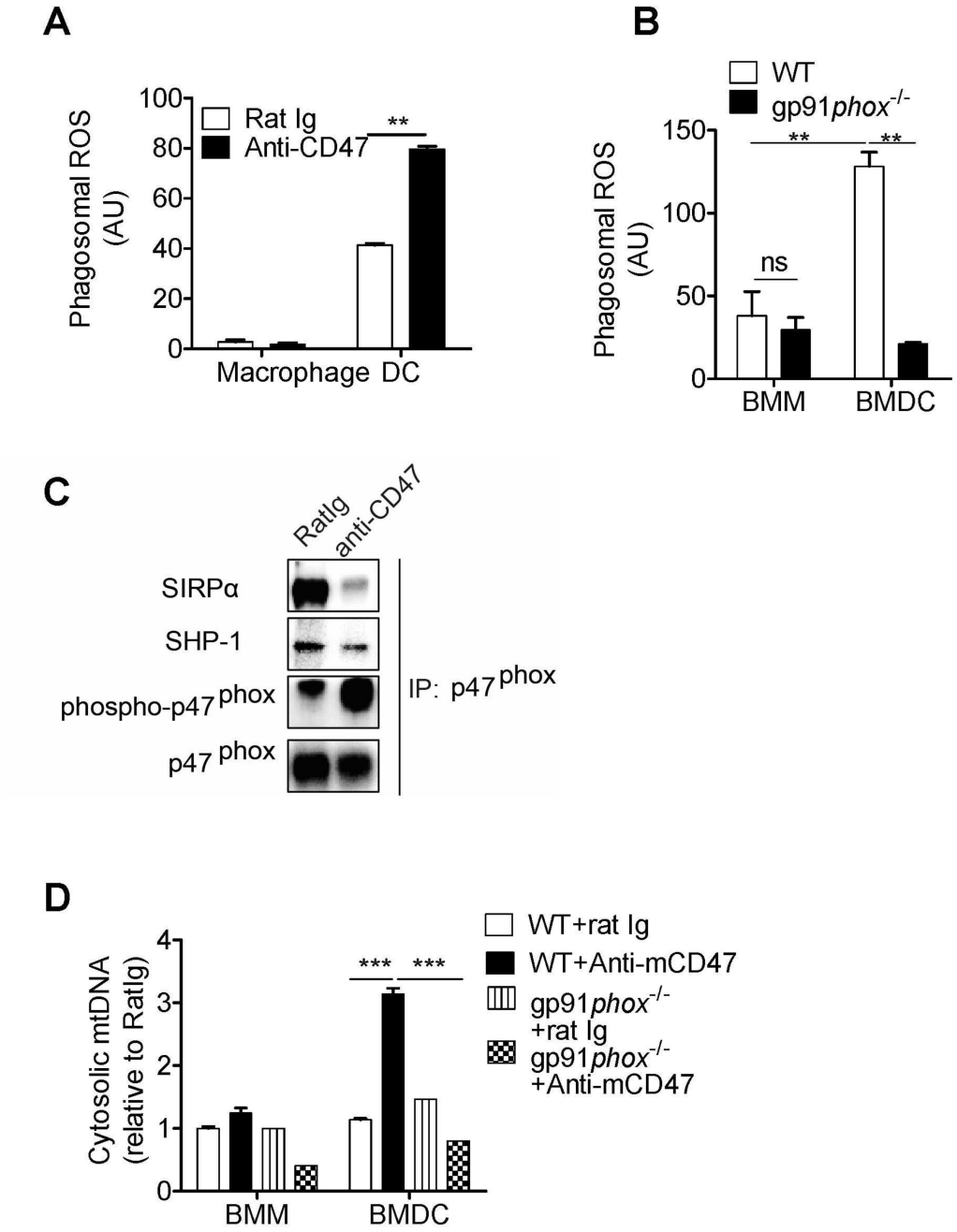

Figure 5. Blocking SIRPα signaling in DCs inhibits the clearance of engulfed mtDNA by activating NOX2

(A) MC38 tumor cells were co-cultured with BMDCs or macrophages in the presence of 30μg/ml rat Ig or anti-CD47 mAb. Generation of phagosomal ROS from DCs or macrophages was measured. **(B)** MC38 tumor cells were co-cultured with bone marrow-derived DCs or macrophages from WT or gp91$^{phox-/-}$ mice in the presence of 30μg/ml rat Ig or anti-CD47 mAb. Generation of phagosomal ROS from DCs or macrophages was measured and normalized to cells treated with rat Ig. **(C)** BMDCs were co-cultured with MC38 in the presence of rat Ig or anti-CD47 mAb for four hours. CD11c^{+} DCs were sorted

by FACS and immunoprecipitated with antibody to $p47^{phox}$. Immunoblot analysis of tyrosine-phosphorylated proteins (p-Tyr) of $p47^{phox}$, or total $p47^{phox}$, SIRPα and SHP-1 was shown. **(D)** BMDCs or BMMs from WT or $gp91^{phox-/-}$ mice were co-cultured with MC38 in the presence of rat Ig or anti-CD47 mAb for four hours. Cytosolic DNA was extracted and quantitated. Data are represented as mean ± SEM. *$p< 0.05$, **$p< 0.01$. ns, not significant (Two-tailed student's t test). Data are representative of two independent experiments. See also Figure S4 and Figure S5.

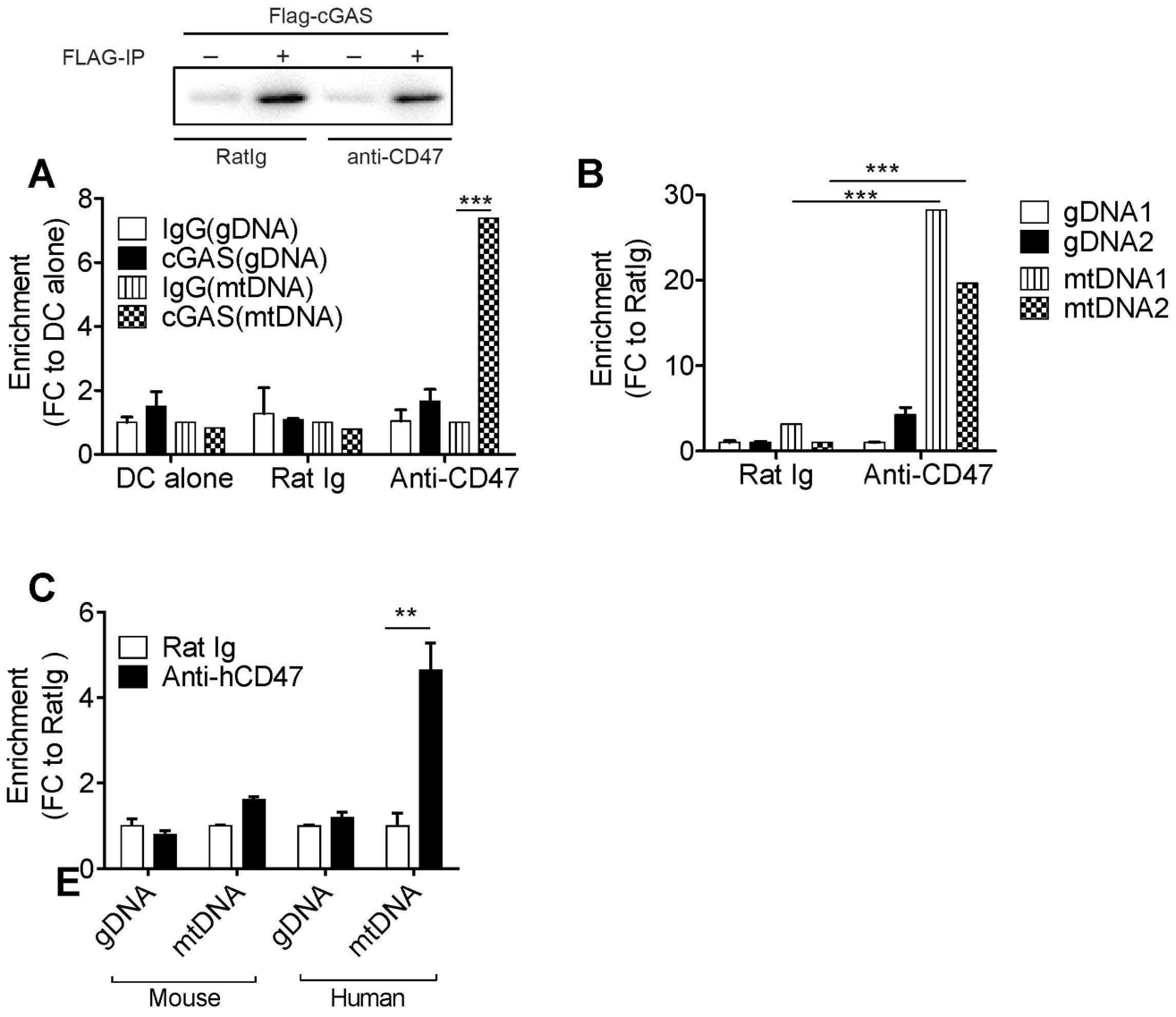

Figure 6. Tumor-originated mtDNA binds directly to cGAS in DC after phagocytosis

(A) DC2.4 was transduced with an expression plasmid encoding FLAG-mouse cGAS and co-cultured with MC38 cells in the presence of 30μg/ml rat Ig or anti-CD47 mAb. Top, lysates taken from purified DC2.4 were immunoprecipitated (IP) with anti-FLAG followed by immunoblot analysis. Bottom, cell lysates were immunoprecipitated with anti-FLAG Ab or isotype Ab. DNA fragments were amplified by real-time qPCR using the primer pair for mtDNA(*nd1*) and the primer pair for gDNA(*PolG1*). **(B)** BMDCs were cultured with MC38 in the presence of 30μg/ml rat Ig or anti-CD47 mAb for eight hours. DCs were purified. Cell lysates were immunoprecipitated with anti-mouse cGAS Ab or isotype Ab. **(C)** BMDCs from NSG mice were cultured with human cell line HCT116 in the presence of 30μg/ml rat Ig or anti-human CD47 mAb (B6H12) for eight hours. $CD11c^+$ DCs were purified. Cell lysates were immunoprecipitated with anti-mouse cGAS Ab or isotype Ab. Data were normalized to the IP isotype for each sample and are expressed as the fold change (FC) in enrichment of DNA. Data are presented as mean ± SEM. $^{**}p < 0.01$, $^{***}p < 0.001$ (Two-

tailed student's t test). Data were representative of three (A and B) or two (C) independent experiments.

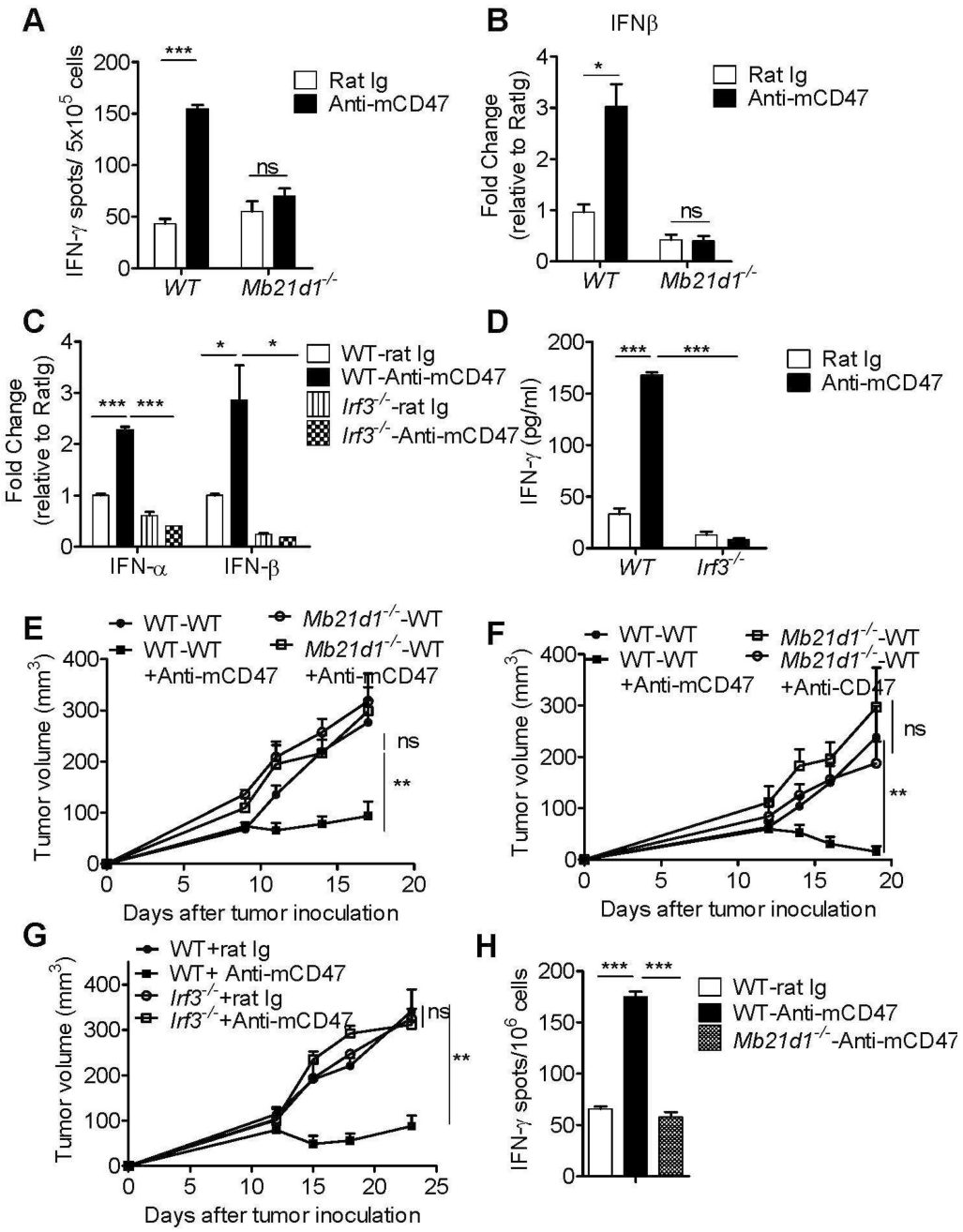

Figure 7. CD47 blockade triggers cGAS-STING-IRF3-mediated innate sensing in DC

(A) BMDCs isolated from wild-type mice (WT) or *Mb21d1*$^{-/-}$ mice were cultured with B16-OVA tumor cells in the presence of rat Ig or anti-CD47 mAb for 16 hours. Subsequently, purified CD11c^{+} cells were co-cultured with OT-I T cells for two days and the IFN-γ production was analyzed by ELISPOT assays. **(B)** BMDCs isolated from wild-type (WT) mice or cGAS$^{-/-}$ mice were cultured with B16-OVA tumor cells in the presence of rat Ig or anti-CD47 mAb for 16 hours. Purified CD11c^{+} cells were evaluated for IFN-β transcripts. **(C–D)** BMDCs from WT or Irf3$^{-/-}$ mice were used for co-culturing with MC38-SIY cells. Type I IFN(IFN-α and IFN-β) production was analyzed by real-time PCR assay

(C) and DC cross-priming activity was analyzed by IFN-γ CBA assays (D). **(E–F)** CD45.1 mice were transferred with bone marrow cells (BMC) from WT or *Mb21d1*$^{-/-}$ mice. Six weeks after bone marrow chimera reconstitution, mice were injected s.c. with 1×10^6 MC38 (E) or B16-SIY (F). Tumor-bearing mice were treated i.t. with 50μg anti-CD47 mAb or rat Ig. (E) MC38 tumor growth in WT-WT and *Mb21d1*$^{-/-}$-WT reconstituted mice (n =5 mice/ group). (F) B16-SIY tumor growth in WT-WT and *Mb21d1*$^{-/-}$-WT reconstituted mice (n =5 mice/ group). **(G)** WT mice or *Irf3*$^{-/-}$ mice (n = 5 mice/group) were injected s.c. with 10^6 MC38 cells and treated i.t. with 50 μg of anti-CD47 or rat Ig on days 12 and 15. **(H)** MC38 tumor-bearing BMC reconstituted mice (n = 5 mice/ group) were sacrificed 10 days after anti-CD47 mAb treatment. 2.5×10^5 CD8$^+$ T cells were re-stimulated with MC38 tumor cells. The ratio of CD8$^+$ T cells to MC38 was 20:1. IFN-γ–producing cells were enumerated by ELISPOT assay. Data are presented as mean ± SEM. ** $p< 0.01$, *** $p< 0.001$; ns, not significant (Two-tailed student's t test). Data are representative of three independent experiments. See also Figure S6 and Figure S7.